Campbell P, Morton P, Takeichi T, Salam A, Roberts N, Proudfoot LE, Mellerio JE, Aminu K, Wellington C, Patil SN, **Akiyama M**, Liu L, McMillan JR, Aristodemou S, Ishida-Yamamoto A, Abdul-Wahab A, Petrof G, Fong K, Harnchoowong S, Stone K, Harper JI, McLean WHI, Simpson MA, Parsons M, McGrath JA.	Epithelial inflammation resulting from an inherited loss-of-function mutation in *EGFR*.	**J Invest Dermatol**	134 (10)	2570-8	2014
Ohguchi Y, Nomura T, Suzuki S, Mizuno O, Nomura Y, Nemoto-Hasebe I, Okamoto H, Sandilands A, **Akiyama M**, McLean WH, Shimizu H.	A new filaggrin gene mutation in a Korean patient with ichthyosis vulgaris.	**Eur J Dermatol**	24 (4)	491-493	2014
Muro Y, Tsuchisaka A, Ishii N, Hashimoto T, Sugiura K, **Akiyama M**.	Author's reply to "detection of anti-periplakin autoantibodies during idiopathic pulmonary fibrosis" by Taillé et al.	**Clin Chim Acta**	433	194	2014

Sugiura K, Oiso N, Iinuma S, Matsuda H, Minami-Hori M, Ishida-Yamamoto A, Kawada A, Iizuka H, **Akiyama M**.	*IL36RN* mutations underlie impetigo herpetiformis.	**J Invest Dermatol**	134 (9)	2472-2474	2014
Ogawa M, **Akiyama M**.	Successful topical adapalene treatment for the facial lesions of an adolescent case of epidermolytic ichthyosis.	**J Am Acad Dermatol**	71 (3)	e103-5	2014
Mizuno O, Nomura T, Suzuki S, Takeda M, Ohguchi Y, Fujita Y, Nishie W, Sugiura K, **Akiyama M**, Shimizu H.	Highly prevalent SERPINB7 founder mutation causes pseudodominant inheritance pattern in Nagashima-type palmoplantar keratosis.	**Br J Dermatol**	171	847-853	2014
Sugiura K, Suga Y, **Akiyama M**.	Dorfman-Chanarin syndrome without mental retardation caused by a homozygous ABHD5 splice site mutation that skips exon 6.	**J Dermatol Sci**	75 (3)	199-201	2014
Mizutani K, Taira M, **Akiyama M**.	Primary mucinous carcinoma of the skin on the breast with lymph node metastasis.	**J Dermatol**	41 (8)	760-761	2014

Ito E, Muro Y, Sugiura K, **Akiyama M**.	Hydroxyurea-induced amyopathic dermatomyositis presenting with heliotrope erythema.	**Dermatology Online J**	20 (8)	pii: 13030/qt2r11f768. http://www.escholarship.org/uc/item/2r11f768.	2014
Muro Y, Sugiura K, **Akiyama M**.	Is the measurement of anti-PM-1 α antibodies at least as important as that of other systemic sclerosis-specific antibodies? Comment on the article by D'Aoust et al.	**Arthritis Rheumatol**	66 (11)	3248	2014
Sugiura K, Uchiyama R, Okuyama R, **Akiyama M**.	Varicella zoster virus-associated generalized pustular psoriasis in a baby with heterozygous IL36RN mutation.	**J Am Acad Dermatol**	71	e216-218	2014

Petrof G, Nanda A, Howden J, Takeichi T, McMillan JR, Aristodemou S, Ozoemena L, Liu L, South AP, Pourreyron C, Dafou D, Proudfoot LE, Al-Ajmi H, **Akiyama M**, McLean WHI, Simpson MA, Parsons M, McGrath JA.	Mutations in *GRHL2* result in an autosomal-recessive ectodermal dysplasia syndrome.	**Am J Hum Genet**	95 (3)	308-14	2014
Saito K, Ito A, Ishikawa K, Shimada H, Takeo N, Hatano Y, Sugiura K, **Akiyama M**, Inomata M, Kitano S, Fujiwara S.	Pustular psoriasis occurring after total colectomy for ulcerative colitis and relieved by administration of infliximab.	**J Dermatol**	41 (11)	1033-1034	2014
Muro Y, Nakashima R, Hosono Y, Sugiura K, Mimori T, **Akiyama M**.	Autoantibodies to DNA mismatch repair enzymes in polymyositis/dermatomyositis and other autoimmune diseases: a possible marker of favorable prognosis.	**Arthritis Rheumatol**	66 (12)	3457-3462	2014

Shimizu Y, Ogawa Y, Sugiura K, Takeda J, Sakai-Sawada K, Yanagi T, Kon A, Sawamura D, Shimizu H, **Akiyama M**.	A palindromic motif in the -2084 to -2078 upstream region is essential for ABCA12 promoter function in cultured human keratinocytes.	**Sci Rep**	4	6737	2014
Nakazawa M, Akasaka M, Hasegawa T, Suzuki T, Shima T, Takanashi JI, Yamamoto A, Ishidou Y, Kikuchi K, **Niijima S**, Shimizu T, Okumura A.	Efficacy and safety of fosphenytoin for acute encephalopathy in children.	**Brain Dev**		pii: S0387-7604(14)00157-0	2014
Sugano H, Nakanishi H, Nakajima M, Higo T, Iimura Y, Tanaka K, Hosozawa M, **Niijima S**, Arai H.	Posterior quadrant disconnection surgery for Sturge-Weber syndrome.	**Epilepsia**	55	683-9	2014
Ihara N, **Umezawa A**, Onami N, Tsumura H, Inoue E, Hayashi S, Sago H, Mizutani S.	Partial rescue of mucopolysaccharidosis type VII mice with a lifelong engraftment of allogeneic stem cells in utero.	**Congenit Anom.**	55	55-64	2015

Inoue T, **Umezawa A**, Takenaka T, Suzuki H, Okada H.	The contribution of epithelial-mesenchymal transition to renal fibrosis differs among kidney disease models.	**Kidney Int.**	87	233-238	2015
Higuchi A, Ling QD, Kumar SS, Munusamy MA, Alarfaj AA, Chang Y, Kao SH, Lin KC, Wang HC, **Umezawa A**.	Generation of pluripotent stem cells without the use of genetic material.	**Lab Invest.**	95	26-42	2015
Santostefano KE, Hamazaki T, Biel NM, Jin S, **Umezawa A**, Terada N.	A practical guide to induced pluripotent stem cell research using patient samples.	**Lab Invest.**	95	4-13	2015
Lu S, Kanekura K, Hara T, Mahadevan J, Spears LD, Oslowski CM, Martinez R, Yamazaki-Inoue M, Toyoda M, Neilson A, Blanner P, Brown CM, Semenkovich CF, Marshall BA, Hershey T, **Umezawa A**, Greer PA, Urano F.	A calcium-dependent protease as a potential therapeutic target for Wolfram syndrome.	**Proc Natl Acad Sci U S A.**	111	E5292-301	2014

Aino M, Nishida E, Fujieda Y, Orimoto A, Mitani A, Noguchi T, Makino H, Murakami S, **Umezawa A**, Yoneda T, Saito M.	Isolation and characterization of the human immature osteoblast culture system from the alveolar bones of aged donors for bone regeneration therapy.	**Expert Opin Biol Ther**.	14	1731-1744	2014
Fukuda A, Tomikawa J, Miura T, Hata K, Nakabayashi K, Eggan K, Akutsu H, **Umezawa A**.	The role of maternal-specific H3K9me3 modification in establishing imprinted X-chromosome inactivation and embryogenesis in mice.	**Nat Commun**.	5	5464	2014
Okamoto N, Aoto T, Uhara H, Yamazaki S, Akutsu H, **Umezawa A**, Nakauchi H, Miyachi Y, Saida T, Nishimura EK.	A melanocyte--melanoma precursor niche in sweat glands of volar skin.	**Pigment Cell Melanoma Res**.	27	1039-1050	2014

Izumi Y, Suzuki E, Kanzaki S, Yatsuga S, Kinjo S, Igarashi M, Maruyama T, Sano S, Horikawa R, Sato N, Nakabayashi K, Hata K, **Umezawa A**, Ogata T, Yoshimura Y, Fukami M.	Genome-wide copy number analysis and systematic mutation screening in 58 patients with hypogonadotropic hypogonadism.	**Fertil Steril.**	102	1130-1136.e3	2014
Nishi M, Akutsu H, Kudoh A, Kimura H, Yamamoto N, **Umezawa A**, Lee SW, Ryo A.	Induced cancer stem-like cells as a model for biological screening and discovery of agents targeting phenotypic traits of cancer stem cell.	**Oncotarget.**	5	8665-8680	2014
Igawa K, Kokubu C, Yusa K, Horie K, Yoshimura Y, Yamauchi K, Suemori H, Yokozeki H, Toyoda M, Kiyokawa N, Okita H, Miyagawa Y, Akutsu H, **Umezawa A**, Katayama I, Takeda J.	Removal of reprogramming transgenes improves the tissue reconstitution potential of keratinocytes generated from human induced pluripotent stem cells.	**Stem Cells Transl Med.**	3	992-1001	2014

Kami D, Kitani T, Kishida T, Mazda O, Toyoda M, Tomitaka A, Ota S, Ishii R, Takemura Y, Watanabe M, **Umezawa A**, Gojo S.	Pleiotropic functions of magnetic nanoparticles for ex vivo gene transfer.	**Nanomedicine**.	10	1165-1174	2014
Ichida JK, T C W J, Williams LA, Carter AC, Shi Y, Moura MT, Ziller M, Singh S, Amabile G, Bock C, **Umezawa A**, Rubin LL, Bradner JE, Akutsu H, Meissner A, Eggan K.	Notch inhibition allows oncogene-independent generation of iPS cells.	**Nat Chem Biol**.	10	632-639	2014
Fukawatase Y, Toyoda M, Okamura K, Nakamura K, Nakabayashi K, Takada S, Yamazaki-Inoue M, Masuda A, Nasu M, Hata K, Hanaoka K, Higuchi A, Takubo K, **Umezawa A**.	Ataxia telangiectasia derived iPS cells show preserved x-ray sensitivity and decreased chromosomal instability.	**Sci Rep**.	4	5421	2014

Author Summary

Loss of gene functions due to nonsense mutations is a typical pathogenic mechanism of hereditary diseases. They may, however, in certain genetic contexts, confine the effects of other dominant pathogenic mutations and suppress disease manifestations. We report the first instance in the literature where the reversion of a "confining" nonsense mutation in *GJB2* gene released the dominant pathogenic effect of a coexsisting gain-of-function mutation, eliciting the lethal form of keratitis-ichthyosis-deafness syndrome (KID). We describe this form of KID syndrome caused by the reversion of the *GJB2* nonsense mutation p.Tyr136X that would otherwise have confined the effect of another dominant lethal mutation, p.Gly45Glu, in the same allele. The patient's mother had the identical misssense mutation which was confined by the nonsense mutation. An epidemiologic estimation demonstrates that approximately 11,000 individuals in the Japanese population may have the same lethal *GJB2* mutation, nonetheless protected from the manifestation of the syndrome because they also inherit the common "confining" nonsense mutation. The reversion-triggered onset of the disease shown in this study is a previously unreported genetic pathogenesis based on Mendelian inheritance.

at birth, and later she developed typical manifestations that lead to the diagnosis of KID syndrome (Figure 1A). Despite intensive care, she died of the disease.

Sequence analysis of *GJB2* was performed to confirm the diagnosis. Direct sequencing of PCR fragments spanning all the exons of *GJB2* revealed a heterozygous missense mutation, c.134G>A (p.Gly45Glu), in exon 2 of *GJB2* in the patient and her mother, but not in her father (Figure 1B). Her mother had an additional heterozygous nonsense mutation, c.408C>A (p.Tyr136X), in the same exon (Figure 1B). TA cloning analysis showed that the c.408C>A and c.134G>A mutations were in cis configuration. All family members uniformly harbored the two known non-pathological SNPs [5] c.79G>A (p.Val27Ile) (rs2274084) and c.341A>G (p.Glu114Gly) (rs2274083) heterozygously and in trans configuration with the c.134G>A or c.408C>A mutation (Figure 1C and 2A). The existence of the *GJB2* mRNA harboring the c.134G>A missense mutation in the patient's skin was verified by a RT-PCR assay (Figure S1). To confirm the biological relationship between the patient and her parents, we genotyped for 15 short tandem repeat (STR) loci with tetranucleotide repeat units using a multiplex kit. Since all of the genotypes for 15 STR loci were consistent with the relationship between the parents and child and each combined probability of exclusion and paternity was calculated as 0.999999997 and 0.9999999986, respectively, the authenticity of biological relationship between the parents and the child was confirmed accurately (Tables S1 and S2).

Revertant Mutation of Confining Nonsense Mutation Occurred in the Patient's Pathogenic Allele of *GJB2*

To elucidate the origin of the c.134G>A mutation in the patient, haplotype analysis was performed. Forty SNPs annotated by the International HapMap Project [6] spanning the >39 kbp region surrounding the *GJB2* gene were sequenced. Fourteen SNPs were found to be heterozygous in one or more of the family members (Figure 1C and S2). TA cloning analysis mapped the heterozygous SNPs into three separate genetic regions (Figure 1C). All family members had at least one common haplotype in each genetic region, suggesting that they share a haplotype in the > 39 kb genetic region we studied. Unexpectedly, the patient harbored a unique haplotype that was not seen in either of her parents (Figure 1C). No evidence of spontaneous mutations was found besides these SNP sites through the direct sequencing of the entire coding region of *GJB2*.

We performed an extended SNP microarray analysis spanning 83,483 SNPs throughout chromosome 13. No apparent chromosomal aberration was detected besides a 1,430 kbp copy-number neutral loss-of-heterozygosity region on 13q31.1 which was unique to the patient's genome.

From these findings, we reasoned that an allelic recombination event involving the shared allele (Figure 1C, shown in blue) and the maternally unique allele (Figure 1C, shown in orange) generated the haplotype unique to the patient (see also the Discussion section below), since it differs by three or more base pairs from the counterparts carried by either parent, giving only a remote possibility of coincidental accumulation of spontaneous point mutations at these specific SNP sites. The latter possibility, however, cannot be completely excluded.

The blood cells of the patient did not show mosaicism, and the patient's skin symptoms were fairly evenly distributed over the entire body surface. These findings suggest that the patient was not mosaic for the *GJB2* mutation. Thus, we consider the reversion leading to the pathogenic allele in the patient to be a pre-zygotic event.

Gap Junctions Containing p.Gly45Glu-Mutant Connexin 26 (CX26) Showed Aberrant Gating Activity, Whereas p.Gly45Glu/p.Tyr136X-Mutant CX26 Were Excluded from Functional Gap Junction Formation

As described above, the patient who harbored the p.Gly45Glu mutation manifested the disease, while the mother who harbored the mutations p.Gly45Glu and p.Tyr136X was apparently unaffected (Figure 2A). A heterozygous *de novo* p.Gly45Glu mutation is known to cause the lethal form of KID syndrome [3], and its molecular pathogenic mechanism has been well described [7–9]. Cx26, the product of *GJB2*, is a gap junction protein with four transmembrane domains and two extracellular domains (Figure 2B). The Cx26 molecule is a protomer of a hexameric connexon, and two connexons expressed on the membranes of neighboring cells connect to form a gap junction channel [10]. Gly45 locates at a domain that lines the channel pore and probably mediates voltage sensing [10]. Connexons containing p.Gly45Glu mutants function as hemichannels with aberrantly increased activity [7,8] that leads to the disease manifestations [3,9]. It is also known that, besides KID syndrome, biallelic loss of function of *GJB2* causes autosomal recessive non-syndromic hearing loss (NSHL) [11]. The fact that the p.Gly45Glu/p.Tyr136X mutation homozygously or compound heterozygously causes NSHL suggests that this mutation leads to total loss of function for the *GJB2* product [5].

These considerations lead us to hypothesize that the p.Tyr136X mutation confines and rescues the dominant pathogenic effect of the p.Gly45Glu mutation. Since inter-protomer interactions of Cx26 require the fourth transmembrane domain [10] that is terminated by the p.Tyr136X mutation (Figure 2 A and B), a Cx26 carrying p.Gly45Glu/p.Tyr136X alteration would be excluded from the hexameric connexons.

This phenomenon, in which a second-site mutation cancels an exsisting pathogenic mutation, was previously reported; it is called "partial reversion", because the wild-type allele itself is not

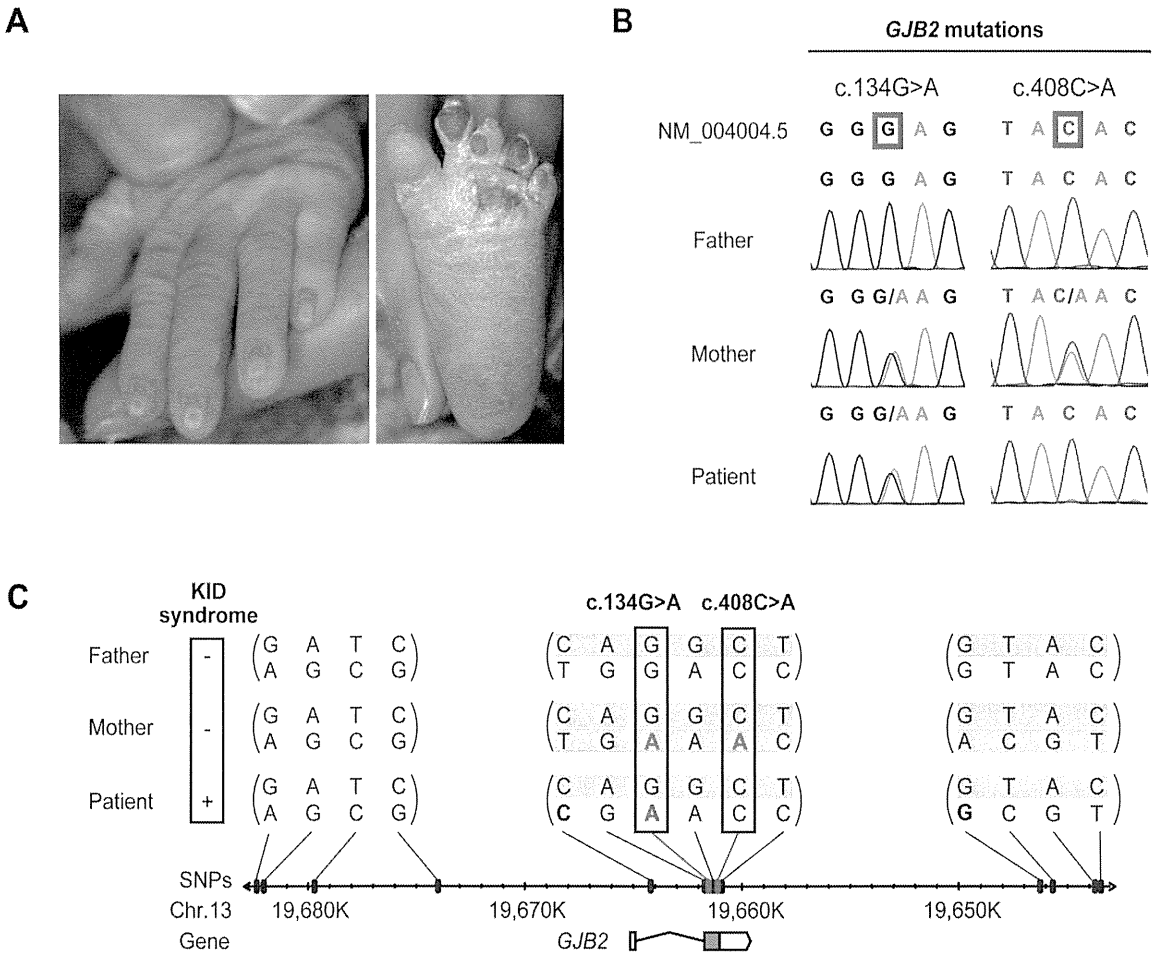

Figure 1. Sequence and haplotype analysis of the present case of KID syndrome. (A) Clinical manifestations of the patient are shown. Marked hyperkeratosis of the palms and soles is seen. (B) Identification of c.134G>A and c.408C>A mutations in the patient and her parents. The patient is compound heterozygous for the two mutations. (C) Haplotype analysis of the family members. Fourteen heterozygous SNPs spanning > 39 kbp surrounding the *GJB2* gene are identified and assembled into three contigs (shown in parenthesis). The nucleotides altered by the c.134G>A and c.408C>A mutations are boxed. The altered nucleotides are in red. The patient and her parents share a single haplotype (top; blue background). The patient has a unique haplotype (bottom; yellow background) that is not harbored by either parent. The maternally unique haplotype is shown in orange.

doi:10.1371/journal.pgen.1004276.g001

attained, although the seoncd-site mutation rescues the disease [12].

To test this hypothesis, we observed the colocalization of fluorescent-tagged Cx26 variants in HeLa cells. The father had wild-type and p.Val27Ile/p.Glu114Gly variant alleles (Figure 2A). When these Cx26s were cotransfected, they together formed gap junctions, suggesting that both proteins retain their native functions (Figure 3A). The Cx26 p.Gly45Glu/p.Tyr136X mutant failed to enter the gap junction generated by Cx26 p.Val27Ile/p.Glu114Gly, demonstrating that only the latter form comprises the functional gap junctions in the mother (Figure 3A). Cx26 p.Gly45Glu colocalized with the p.Val27Ile/p.Glu114Gly variant but failed to form gap junctions (Figure 3A). In a neurobiotin uptake assay, which monitors channel activity as cellular uptake of a neurobiotin tracer [9], only the p.Gly45Glu mutant and not the p.Gly45Glu/p.Tyr136X mutant induced the aberrant uptake (Figure 3B).

Discussion

Many cases of revertant mosaicism have been reported as "natural gene therapy" where the mitotic recombination results in revertant mutations that mitigate the disease symptoms [13–16]. However, the present study is the first report to demonstrate a mutant reversion triggering a genetic disease.

The present data of genomic DNA sequencing and haplotype analysis demonstrate that the patient and her father share an identical haplotype (Figure 1C, shown in blue). We hypothesized that the entire blue allele in the patient's genome was derived from the father, while the other allele (Figure 1C, shown in yellow) was basically derived from the mother. It seemed, however, that this allele underwent pre-zygotic reversion during meiosis of the maternal gamete. The fact that the patient's unique allele (Figure 1C, shown in yellow) differs by three non-continuous SNPs from the unique maternal allele (Figure 1C, shown in orange) while the neighboring SNPs are conserved might be explained by multiple events of gene conversion involving both of the maternal alleles (Figure 1C, shown in blue and orange) that may have occurred in this genetic region.

Double cross-over also might account for the recombination, but it is less likely, considering that the non-conserved and conserved SNPs in the patient's allele reside within close proximity (Figure 1C); the average length of the gene conversion tract is estimated to be in the range of 55–290 bp, whereas the cross-over tracts are typically longer [17].

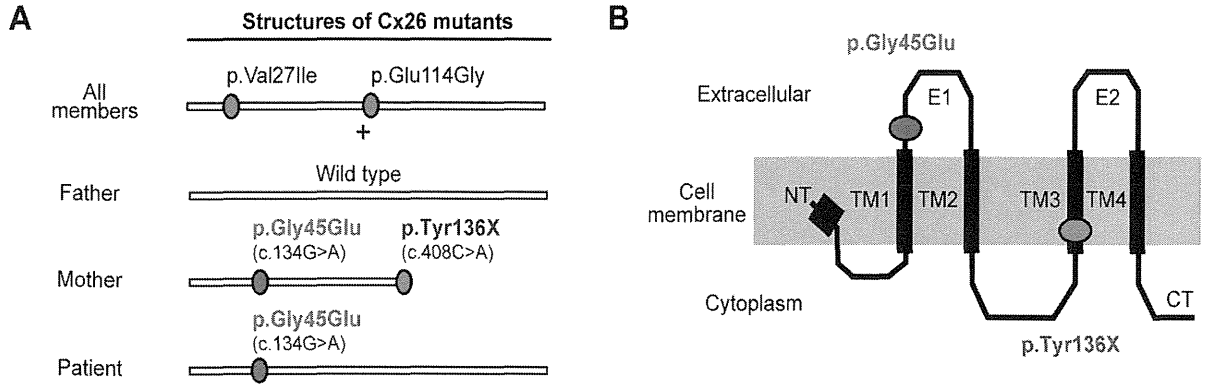

Figure 2. Configurations and topological mapping of the *GJB2* mutations in the family. (A) Structures of Cx26 mutants. The mutations/variants found in each allele of the family members are shown. p.Val27Ile and p.Glu114Gly are non-pathological variants. (B) Topological mapping of the Cx26 mutations. p.Gly45Glu (red) is located in the first extracellular loop domain and is thought to affect the channel activity of gap junctions. TM1–4: transmembrane domain 1–4; E1–2: extracellular domain 1–2; NT: N terminus; CT: C terminus.
doi:10.1371/journal.pgen.1004276.g002

Mitotic gene conversion has been found in some cases of revertant mosaicism in cutaneous disease, including generalized atrophic benign epidermolysis bullosa [12,13]. We are unaware of any previous report of multiple gene conversions within a relatively short genetic segment as in the present case. However, the present data compel us to consider that it occurred. Since the patient's unique allele differs by three or more base pairs from the counterparts carried by either parent, we judge the possibility of coincidental accumulation of spontaneous point mutations at these specific SNP sites to be highly unlikely. This possibility, however, cannot be completely excluded.

As evidence supporting our hypothesis, consistent with a previous report [9], we clearly demonstrated that Cx26 p.Gly45Glu colocalized with the p.Val27Ile/p.Glu114Gly variant but failed to form gap junctions (Figure 3A). Previous studies have shown that Cx26 p.Gly45Glu forms hemichannels that are aberrantly activated at low extracellular Ca2+ levels [9]. The present study used a neurobiotin uptake assay [9] to show that only the p.Gly45Glu mutant and not the p.Gly45Glu/p.Tyr136X mutant induces the aberrant uptake (Figure 3B). These results taken together support the model in which the p.Tyr136X mutation confines the dominant gain-of-function effect of the p.Gly45Glu mutation to prevent the onset of the disease (Figure 4). Such secondary effects of revertants may pose a challenge in genetic analyses of extended genes or more than one gene with functional interactions.

Interestingly, in the group of Japanese patients with bilateral sensorineural hearing loss, it is not uncommon to find *GJB2* p.Gly45Glu carriers, but none of them are affected by KID syndrome [5]. They uniformly have a tandem p.Tyr136X mutation, as in the mother of the present case [5]. Thus, we hypothesized that, in the Japanese population, carriers of p.Gly45Glu are protected from the lethal form of KID syndrome by the tandem, confining mutation p.Tyr136X.

To clarify the frequency of the p.Gly45Glu mutation in the entire Japanese population, we performed screening analysis for the two mutations p.Gly45Glu and p.Tyr136X in a normal control group consisting of 920 overall healthy Japanese individuals (1,840 alleles). Neither p.Gly45Glu nor p.Tyr136X was found in any of the 1,840 alleles (data not shown). Tsukada *et al.* [5] also reported that neither p.Gly45Glu nor p.Tyr136X was found in 252 Japanese healthy control individuals (504 control Japanese alleles). These results indicate that the alleles with tandem p.Gly45Glu and p.Tyr136X mutations are infrequent in the general Japanese population. However, in the epidemiological statistics of Tsukada *et al.* [5], we found screening data for *GJB2* mutations in Japanese patients with sensorineural hearing loss. The report revealed that, among 1,343 Japanese patients with hearing loss, 33 patients had one or two p.Gly45Glu alleles (34 p.Gly45Glu alleles in 2686 alleles for an allele frequency of 1.27%; 33 carriers in 1,343 patients for a carrier rate of 2.46%). This means 2.46% of Japanese patients with bilateral sensorineural hearing loss have one or two p.Gly45Glu alleles. As for the prevalence of sensorineural hearing loss, it was reported that 3.5 per 1,000 individuals in the entire population have bilateral sensorineural hearing loss [18]. Thus, calculating from these epidemiological statistics, we estimate that 8.6 per 100,000 individuals, or approximately 11,000 individuals in the entire Japanese population, have one or two p.Gly45Glu alleles. However, no patient with the lethal form of KID syndrome due to p.Gly45Glu has been reported in the Japanese population as far as we know, although the mutation p.Gly45Glu has been reported as a cause of the lethal form of KID syndrome in several European patients [3,19–22].

Tsukada *et al.* [5] reported that all 34 alleles with p.Gly45Glu found in the Japanese patients with sensorineural hearing loss also had p.Tyr136X, suggesting that p.Gly45Glu is in complete linkage disequillibrium with p.Tyr136X in the Japanese population. In our mutation screening, no allele carrying either or both mutations, p.Gly45Glu and p.Tyr136X, was found in 920 Japanese individuals (1,840 alleles) and these results support the idea that p.Gly45Glu is in complete LD with p.Tyr136X in the Japanese population.

In light of this, we conclude that, even though individuals may have the dominant lethal mutation p.Gly45Glu, the confining mutation p.Tyr136X *in cis* configuration protects against the disease, KID syndrome, in the approximately 11,000 Japanese individuals in the entire Japanese population who harbor p.Gly45Glu. The allele with the tandem mutations p.Gly45Glu and p.Tyr136X causes hearing loss in an autosomal recessive manner. Most carriers of the tandem mutations in the Japanese population are heterozygous for the allele, such as the patient's mother in the present study, and are not affected with hearling loss.

In summary, our findings demonstrate that the second-site confining mutation is an imporatant genetic protection mechanism, and its loss, like the opening of Pandora's box, is a novel genetic pathogenesis that releases the hidden genetic disease.

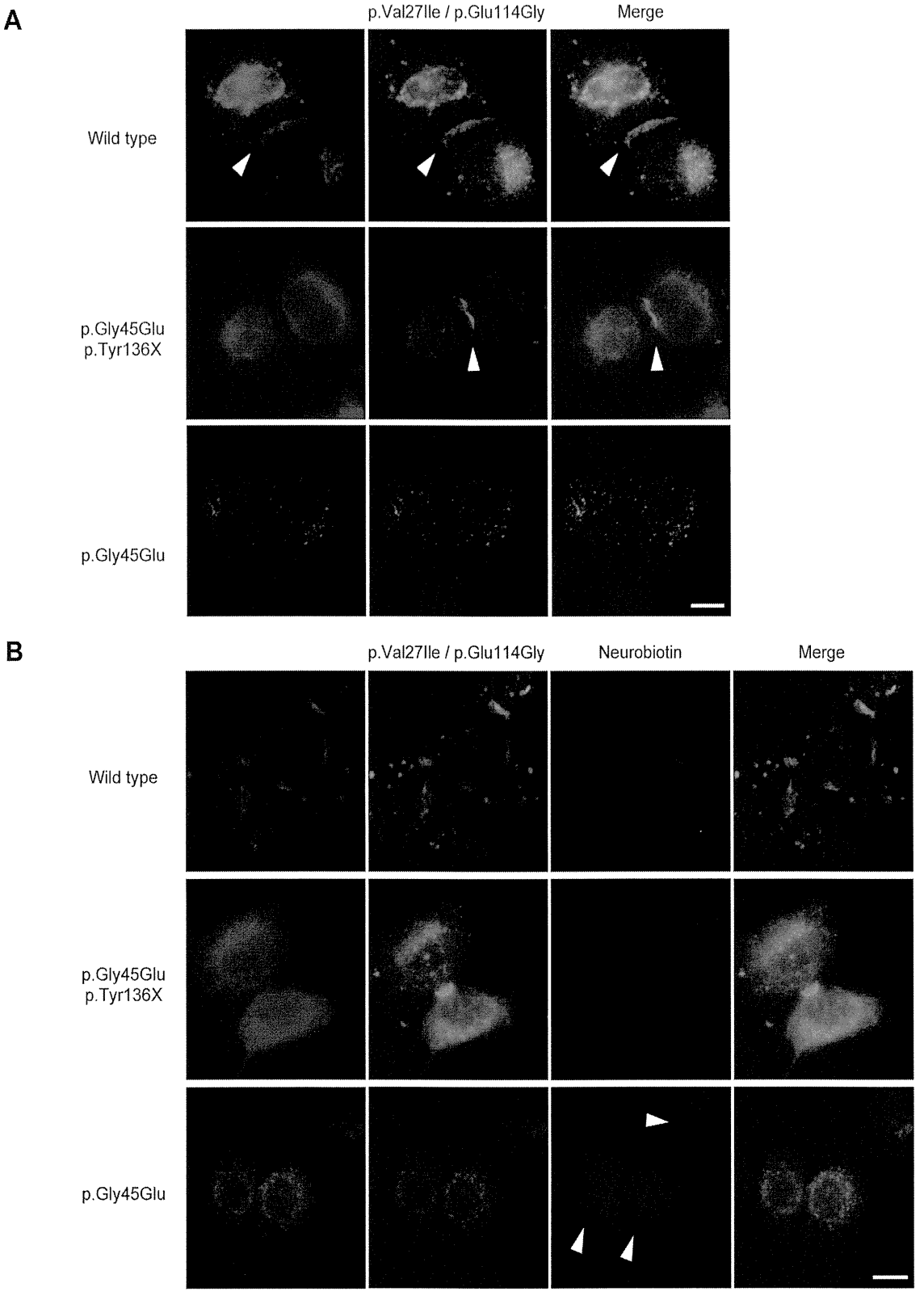

Figure 3. The p.Tyr136X mutation confines the effect of the pGly45Glu mutation. (A) Gap junction formation by the transfected Cx26 variants. Each panel contains two co-transfected cells connected to each other. Wild-type, p.Gly45Glu/p.Tyr136X and p.Gly45Glu mutants of Cx26 were tagged with monomeric Red Fluorescent Protein (mRFP) and co-transfected with Green Fluorescent Protein (EGFP)-tagged Cx26 p.Val27Ile/p.Glu114Gly into HeLa cells as indicated. Gap junction formation sites are indicated by arrowheads. The combination of WT Cx26 and Cx26 p.Val27Ile/p.Glu114Gly (top row) results in gap junctions that consist of both Cx26 proteins (yellow signal). The combination of Cx26 p.Gly45Glu/p.Tyr136X and Cx26 p.Val27Ile/p.Glu114Gly (middle row) results in gap junctions with only Cx26 p.Val27Ile/p.Glu114Gly (green signal). No apparent gap junction formation is seen when Cx26 p.Gly45Glu and Cx26 p.Val27Ile/p.Glu114Gly are cotransfected (bottom row). (B) Aberrant gate opening detected with neurobiotin uptake assay. Fluorescent-tagged Cx26s were cotransfected into HeLa cells as indicated, and treated with neurobiotin in a calcium-free condition. Uptake was detected with AlexaFluor350 streptoavidin dye (blue). Aberrant uptake of neurobiotin is observed only in cells cotransfected with Cx26 p.Gly45Glu and Cx26 p.Val27Ile/p.Glu114Gly (bottom row).
doi:10.1371/journal.pgen.1004276.g003

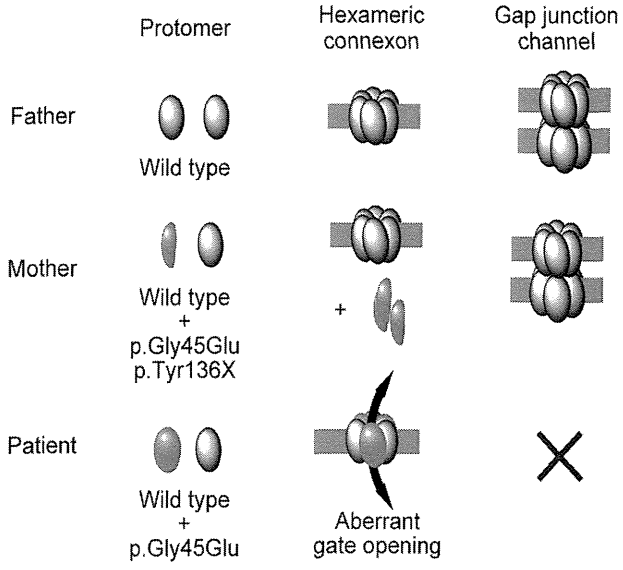

Figure 4. Schematic of the mechanism whereby the p.Tyr136X mutation confines the effect of the p.Gly45Glu mutation. The truncated Cx26 peptides produced from the mutant p.Gly45Glu/p.Tyr136X are not incorporated into connexons or gap junctions (middle row), although Cx26 peptides derived from the mutant p.Gly45Glu are incorporated into connexons, resulting in aberrant gate opening and malformation of gap junctions (bottom row).
doi:10.1371/journal.pgen.1004276.g004

Materials and Methods

Ethics Statement

This study was approved by the Bioethics Committee of the Nagoya University Graduate School of Medicine and was conducted according to The Declaration of Helsinki Principles. Written informed consent was obtained from the parents.

The Patient and Her Parents

The patient was referred and seen at the Outpatient Clinic of Dermatology, Nagoya University Hospital.

Sequence Analysis and TA Cloning

Genomic DNA extracted from peripheral blood was used as a template for PCR amplification, followed by direct automated sequencing. The entire coding regions of *GJB2* including the exon/intron boundaries were sequenced as reported elsewhere [4]. TOPO-TA cloning kit (Life Technologies) was used for TA cloning analyses. PCR primers were designed to amplify the genetic regions containing the selected SNPs, and the acquired PCR products were analyzed by direct sequencing. For amplification of PCR fragments longer than 1,000 base pairs, KOD-Plus-Neo polymerase (Toyobo) or PrimeScript GXL polymerase (Takara Bio) was used and the PCR products were cloned with the TOPO XL-TA Cloning Kit (Life Technologies) after the addition of a 3′-adenine overhang.

Verification of the Parent-Child Relationship

The parent-child relationship was validated using AmpFlSTR Identifier plus PCR amplification kit (Applied Biosystems) according to the manufacturer's instructions. The combined probability of exclusion and the combined probability of paternity (in the case of the odds ratio for prior probability = 1) for 15 STR loci were calculated to confirm the authenticity of the biological relationship between the parents and the child.

Genotyping of *GJB2* Mutations in 920 Japanese Control Individuals

Genomic DNA was extracted from whole blood using the QIAamp DNA Blood Maxi Kit (Qiagen). Real-time PCR-based genotyping of the *GJB2* mutations was performed with TaqMan MGB probe genotyping assay according to the manufacturer's instructions provided by Roche Diagnostics. To detect an allele of each mutation, a set of two TaqMan MGB probes labeled with a fluorescent dye (FAM or VIC) and a quencher dye (non-fluorescent dye; NFD) followed by minor groove binder (MGB), and sequence-specific forward and reverse primers were synthesized by Life Technologies Corporation. The sequences of assay probes/primers are shown in Table S3 in this article's supplementary material. Real-time PCR was performed with LightCycler 480 system II 384 plate (Roche Diagnostics) in a final volume of 5 μl containing 2× LightCycler 480 Probes Master (Roche Diagnostics), 200 nM probes for wild type and mutant each and 900 nM forward and reverse primers each, with 5 ng genomic DNA as the template. The thermal conditions were the following: 95°C for 10 min, followed by 45 cycles of 95°C for 10 s, 60°C for 60 s and 72°C for 1 s, with a final cooling at 40°C for 30 s. Endpoint fluorescence was measured for each sample well. Afterward, genotyping was performed using endpoint genotyping analysis in LightCycler 480 software.

Eight hundred and twenty controls were analyzed with the real-time PCR-based genotyping of *GJB2* mutations, and another 100 controls were analyzed with the direct automated sequencing for the entire coding region of *GJB2*.

GJB2 Expression Study

Total RNA from the formaldehyde-fixed paraffin-embedded skin sample of the patient was extracted using the RNeasy FFPE kit (Qiagen) and Deparaffinization Solution (Qiagen) according to the manufacturer's instructions. The total RNA was reverse-transcribed with a *GJB2* specific primer, 5′-GGATGTGGGAGATGGGGAAGTAGTG-3′, using PrimeScriptII 1st strand cDNA synthesis kit (Takara, Japan). The PCR fragment harboring c.134G>A mutation was amplified with primer sets, 5′-GGAAAGATCTGGCTCACCGTCCTC-3′ and 5′-CGTAGCACACGTTCTTGCAGCCTG-3′, and directly sequenced with the same primers.

SNP Array

Chromosome-wide genotyping was performed using HumanOmni2.5–8 BeadChip (Illumina), which covers a total of 2,379,855 SNPs throughout the genome, including 83,482 SNPs on chromosome 13. Genomic DNA was hybridized according to the manufacturer's instructions and data analysis was carried out using GenomeStudio software (Illumina).

Cell Culture

HeLa cells were cultured in Dulbecco's modified Eagle's medium (DMEM) containing 10% fetal calf serum. For transfection of plasmids, cells were seeded onto 8-well LabTek chamber slides (Thermo Scientific) and transfected with FuGene HD Transfection Reagent (Roche Applied Science) according to the manufacturer's instructions.

Plasmid Construction

The coding sequences of Cx26 variants were amplified from the genome of the patient or the parents, fused to cDNAs coding enhanced green fluorescent protein (EGFP) (Clontech) or monomeric red fluorescent protein (Clontech), and subcloned into

pcDNA3.1(-) plasmid using the InFusion HD Cloning Kit (Takara Bio). The coding sequences of the generated vectors were checked for PCR errors by direct sequencing.

Colocalization Assay

HeLa cells were cotransfected with the EGFP-tagged and mRFP-tagged vectors. Forty-eight hours after transfection, the cells were fixed with 4% formaldehyde. Fluorescent images were obtained using FSX-100 microscope system (Olympus).

Neurobiotin Uptake Assay

HeLa cells were cotransfected with EGFP-tagged and mRFP-tagged Cx26 variant expressing vectors, and neurobiotin uptake assay was performed as described elsewhere [9]. Briefly, cells were washed with calcium free Hank's buffered salt solution for 20 minutes and incubated with phosphate-buffered saline (PBS) containing 0.1 mg/ml neurobiotin (Vector Laboratories) for another 20 minutes. Cells were washed three times with PBS supplemented with 2 mM $CaCl_2$ for 10 minutes at 37°C. The cells were fixed with 4% formaldehyde and permeabilized and blocked with 3% BSA/0.1% Triton X-100/PBS for 1 hour. Then the cells are stained with 3% BSA/0.1% Triton X-100/PBS containing 10 μg/ml Alexa Fluor 350-streptoavidin (Life Technologies) for 1 hour, followed by three washes with 0.1% Triton X-100/PBS. Stained cells were fixed with ProLong Gold antifade reagent (Life Technologies) and fluorescent images were obtained.

Supporting Information

Figure S1 The *GJB2* mRNA harboring the missense mutation is expressed in the patient's skin. (A) RT-PCR from the total RNA extracted from a formaldehyde-fixed paraffin-embedded skin sample of the patient. A 136-bp PCR fragment was amplified from the *GJB2* cDNA obtained from the skin sample of the patient. (B) Detection of *GJB2* cDNA harboring the c.134G>A missense mutation. The PCR fragment was directly sequenced to confirm the expression of the mutant *GJB2* mRNA.
(TIF)

Figure S2 Summary of 40 SNPs spanning the >39 kbp region including GJB2. The SNPs inside the red box reside within the GJB2 gene. Note that the nucleotides are in the strand opposite those shown in Figure 1.
(TIF)

Table S1 Genotyping of the patient and her parents for 15 short tandem repeat (STR) loci.
(DOCX)

Table S2 The combined probability of exclusion and the combined probability of paternity.
(DOCX)

Table S3 The sequence of probes/primers for real-time PCR-based genotyping of *GJB2* mutations.
(DOCX)

Acknowledgments

We thank Professor Akimichi Morita and Dr. Emi Nishida for clinical information. We also thank Dr. Atsushi Enomoto and Kaori Ushida for technical assistance.

Author Contributions

Conceived and designed the experiments: YO KS MA. Performed the experiments: YO TT MK TY. Analyzed the data: YO KS TT MK TY MA. Contributed reagents/materials/analysis tools: NH. Wrote the paper: YO MK.

References

1. Skinner BA, Greist MC, Norins AL (1981) The keratitis, ichthyosis, and deafness (KID) syndrome. Arch Dermatol 117: 285–289.
2. Richard G, Rouan F, Willoughby CE, Brown N, Chung P, et al. (2002) Missense mutations in GJB2 encoding connexin-26 cause the ectodermal dysplasia keratitis-ichthyosis-deafness syndrome. Am J Hum Genet 70: 1341–1348.
3. Janecke AR, Hennies HC, Gunther B, Gansl G, Smolle J, et al. (2005) GJB2 mutations in keratitis-ichthyosis-deafness syndrome including its fatal form. Am J Med Genet A 133A: 128–131.
4. Arita K, Akiyama M, Aizawa T, Umetsu Y, Segawa I, et al. (2006) A novel N14Y mutation in Connexin26 in keratitis-ichthyosis-deafness syndrome: analyses of altered gap junctional communication and molecular structure of N terminus of mutated Connexin26. Am J Pathol 169: 416–423.
5. Tsukada K, Nishio S, Usami S (2010) A large cohort study of GJB2 mutations in Japanese hearing loss patients. Clin Genet 78: 464–470.
6. The International HapMap Consortium (2003) The International HapMap Project. Nature 426: 789–796.
7. Stong BC, Chang Q, Ahmad S, Lin X (2006) A novel mechanism for connexin 26 mutation linked deafness: cell death caused by leaky gap junction hemichannels. Laryngoscope 116: 2205–2210.
8. Gerido DA, DeRosa AM, Richard G, White TW (2007) Aberrant hemichannel properties of Cx26 mutations causing skin disease and deafness. Am J Physiol Cell Physiol 293: C337–345.
9. Mese G, Sellitto C, Li L, Wang HZ, Valiunas V, et al. (2011) The Cx26-G45E mutation displays increased hemichannel activity in a mouse model of the lethal form of keratitis-ichthyosis-deafness syndrome. Mol Biol Cell 22: 4776–4786.
10. Maeda S, Nakagawa S, Suga M, Yamashita E, Oshima A, et al. (2009) Structure of the connexin 26 gap junction channel at 3.5 A resolution. Nature 458: 597–602.
11. Kalatzis V, Petit C (1998) The fundamental and medical impacts of recent progress in research on hereditary hearing loss. Hum Mol Genet 7: 1589–1597.
12. Jonkman MF (1999) Revertant mosaicism in human genetic disorders. Am J Med Genet 85: 361–364.
13. Jonkman MF, Scheffer H, Stulp R, Pas HH, Nijenhuis M, et al. (1997) Revertant mosaicism in epidermolysis bullosa caused by mitotic gene conversion. Cell 88: 543–551.
14. Jonkman MF, Castellanos Nuijts M, van Essen AJ (2003) Natural repair mechanisms in correcting pathogenic mutations in inherited skin disorders. Clin Exp Dermatol 28: 625–631.
15. Choate KA, Lu Y, Zhou J, Choi M, Elias PM, et al. (2010) Mitotic recombination in patients with ichthyosis causes reversion of dominant mutations in KRT10. Science 330: 94–97.
16. Kiritsi D, He Y, Pasmooij AM, Onder M, Happle R, et al. (2012) Revertant mosaicism in a human skin fragility disorder results from slipped mispairing and mitotic recombination. J Clin Invest 122: 1742–1746.
17. Jeffreys AJ, May CA (2004) Intense and highly localized gene conversion activity in human meiotic crossover hot spots. Nat Genet 36: 151–156.
18. Morton CC, Nance WE (2006) Newborn hearing screening–a silent revolution. N Engl J Med 354: 2151–2164.
19. Griffith AJ, Yang Y, Pryor SP, Park HJ, Jabs EW, et al. (2006) Cochleosaccular dysplasia associated with a connexin 26 mutation in keratitis-ichthyosis-deafness syndrome. Laryngoscope 116: 1404–1408.
20. Jonard L, Feldmann D, Parsy C, Freitag S, Sinico M, et al. (2008) A familial case of Keratitis-Ichthyosis-Deafness (KID) syndrome with the GJB2 mutation G45E. Eur J Med Genet 51: 35–43.
21. Sbidian E, Feldmann D, Bengoa J, Fraitag S, Abadie V, et al. (2010) Germline mosaicism in keratitis-ichthyosis-deafness syndrome: pre-natal diagnosis in a familial lethal form. Clin Genet 77: 587–592.
22. Koppelhus U, Tranebjaerg L, Esberg G, Ramsing M, Lodahl M, et al. (2011) A novel mutation in the connexin 26 gene (GJB2) in a child with clinical and histological features of keratitis-ichthyosis-deafness (KID) syndrome. Clin Exp Dermatol 36: 142–148.

International Journal of
Dermatology

Report

Proposed classification of longitudinal melanonychia based on clinical and dermoscopic criteria

Masaki Sawada, MD, Kenji Yokota, MD, Takaaki Matsumoto, MD, Shinichi Shibata, MD, Satoshi Yasue, MD, Akihiro Sakakibara, MD, Phd, Michihiro Kono, MD, Phd, and Masashi Akiyama, MD, Phd

Department of Dermatology, Nagoya University Graduate School of Medicine, Nagoya, Japan

Correspondence
Masashi Akiyama, MD
Department of Dermatology
Nagoya University Graduate School of Medicine
65 Tsurumai-cho
Showa-ku
Nagoya, 466-8550
Japan
E-mail: makiyama@med.nagoya-u.ac.jp

Funding: None.
Conflicts of interest: None.

Abstract

Background For longitudinal melanonychia, clinical and dermoscopic criteria for differentiating malignant melanoma *in situ* from benign nevus/lentigo/functional melanonychia have not been fully established.

Objective To propose a clinical classification of longitudinal melanonychia that is useful in judging the need for follow-up.

Methods A total of 137 patients with longitudinal melanonychia referred to our outpatient clinic in the most recent eight years were included. The mean and median lengths of follow-up for patients were 5.0 and 5.5 years, respectively. We classified the 137 lesions into three types by clinical and dermoscopic features of the nail and periungual skin, including Hutchinson sign, variation of color, and borders in the pigmentation band. We observed type I and II lesions with dermoscopy every six months and three months, respectively.

Results After follow-up, all 72 lesions classified as type I were thought to be benign nevus/lentigo/functional melanonychia. Five of the 52 lesions classified as type II showed enlargement during follow-up, and biopsy was performed. Of these five lesions, three were diagnosed as nevus/lentigo, and the other two were diagnosed as malignant melanoma *in situ*. All 13 lesions classified as type III were diagnosed as malignant melanoma *in situ*.

Conclusion We can expect a type I lesion to be a benign nevus/lentigo/functional melanonychia and a type III lesion to be a malignant melanoma *in situ*; however, type II lesions fall in a gray zone. We believe this classification is useful in deciding treatment and follow-up.

Introduction

Melanonychia, a brown or black pigmentation of the nail plate, can result from not only melanin deposition but also subungual bleeding, bacterial or fungal infection, etc.[1] Melanonychia resulting from melanin deposition commonly appears as a longitudinal band (longitudinal melanonychia, LM) that starts from the matrix and extends to the tip of the nail plate.[2,3] The main challenge in managing a patient with LM is to distinguish malignant melanoma (MM) from benign conditions without delay.

There are no evidence-based studies to determine the optimal frequency of dermoscopic follow-up in patients with LM nor to make precise dermoscopic criteria that can be used to decide when to biopsy the LM lesion.[2] In this study toward proposing a useful clinical classification of LM for follow-up, we studied the clinical and dermoscopic features and outcomes of a Japanese cohort of patients with LM retrospectively.

Materials and methods

Patients

We retrospectively examined 137 patients with LM referred to our outpatient clinic in the Department of Dermatology, Nagoya University Hospital (Nagoya, Japan), in the most recent eight years. The mean and median lengths of follow-up for all patients were 5.0 and 5.5 years, respectively. There was no significant difference in the length of follow-up between patients classified as type I and type II. Most of the patients are still being followed up.

We excluded advanced MM with LM lesions. Clinical and dermoscopic images were recorded at the initial visit, and the observed features were recorded without any knowledge of diagnosis. The diagnosis was based on pathologic examination of a representative nail matrix biopsy specimen and/or records of the patient's medical history/course.[4]

We performed whole-lesion excisional biopsy on 18 LM lesions in our cohort, including 15 lesions that were finally

diagnosed as subungual MM *in situ* (MMIS). The other 119 patients with LM were followed up as functional melanonychia, lentigo, or nevus, without biopsy.

Clinical and dermoscopic criteria employed in this study

The three important criteria used in the present study were Hutchinson sign observed by naked eye (presence vs. absence), color variation in the pigmentation band on the nail plate (presence vs. absence), and lines in the pigmentation band (regular vs. irregular) observed dermoscopically (Fig. 1). Both Hutchinson sign and pseudo-Hutchinson sign are macroscopic pigmentation on the periungual skin observable with the naked eye. The present study defines Hutchinson sign as pigmentation on the periungual skin that shows a parallel ridge pattern, an atypical pigment network, and irregular streaks by dermoscopic observation. Pseudo-Hutchinson sign is defined as periungual pigmentation with dermoscopic features of regular fibrillar pattern, lattice-like pattern, parallel furrow pattern, and/or typical pigment network. Micro-Hutchinson sign is defined as pigmentation observed dermoscopically but not by the naked eye. The atypia of the nail plate and the periungual skin pigmentation were evaluated as levels 1–3 according to the criteria shown in Table 1.

Classification methods for longitudinal melanonychia types I–III

We classified LM lesions into three types by clinical and dermoscopic features of the nail and periungual skin. As mentioned above and described in Table 1, the severity of pigmentation atypicalities in the nail plate and periungual skin was classified as level 1, 2, or 3 by clinical and dermoscopic observation. Using the pigmentation atypicality level of both the nail plate and periungual skin, LM lesions were divided into three types (I, II, and III) according to the system described in Figure 2 and outlined as follows. Type I: level 1, pigmentation atypicality in both the nail plate and periungual skin. Type II: level 2, pigmentation atypicality in either or both but no level 3 pigmentation atypicality, and pseudo-Hutchinson sign is not necessary. Type III: level 3, pigmentation atypicality in either or both. Three to six separate expert dermatologists and one dermatopathologist were included in the selection process. The type of lesion that the majority of investigators selected was adopted. The dermatologists involved in this classification procedure were the same as those involved in following up some individual patients. Thus, the study was not blinded.

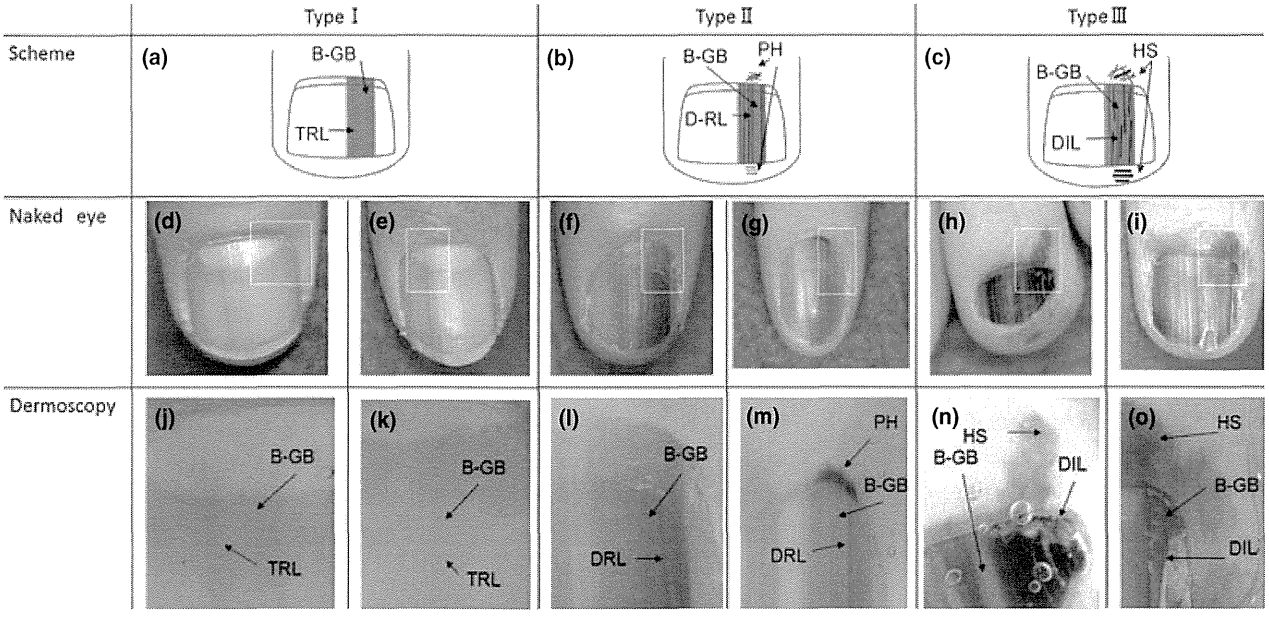

Figure 1 Schematic, clinical, and dermoscopic images showing features of the three types of longitudinal melanonychia (LM). (a,d,e,j,k) Type I LM: a brown or grayish background (B-GB) and a thin regular gray line (TRL) are seen in the nail plate. No pigmentation is apparent in the periungual skin. (b,f,g,l,m) Type II LM: a brown or grayish background (B-GB) and a darker regular gray line (DRL) are observed in the nail plate. Pseudo-Hutchinson sign (PH) with regular fibrillar pattern, lattice-like pattern, parallel furrow pattern, and typical pigment network is sometimes seen in the periungual skin. (c,h,i,n,o) Type III LM: a brown or grayish background (B-GB) and a darker irregular gray line (DIL) are seen in the nail plate. Hutchinson sign or micro-Hutchinson sign (HS) showing parallel ridge pattern, atypical pigment network and irregular streaks is frequently observed in the periungual skin. (a–c) Schematic images showing typical features of type I (a), II (b), and III (c) LM lesions. (d–i) Clinical naked-eye views representing features of type I (d,e), II (f,g), and III (h,i) LM lesions. (j–o) Dermoscopic features corresponding to type I (j,k), II (l,m), and III (n,o) LM lesions. Each rectangle in d–i is enlarged in j–o, respectively

Table 1 Severity of pigmentation atypicalities in longitudinal melanonychia by clinical and dermoscopic observation

	Level 1	Level 2	Level 3
Nail plate	Brown or grayish background with thin regular gray line/almost homogeneous by naked eye)	Brown or grayish background with darker regular line	Brown or grayish background with darker irregular line
Periungual skin	No pigmentation	(Pseudo-Hutchinson sign)[a]	(Micro-) Hutchinson sign

[a]Not required.

Follow-up/treatment for longitudinal melanonychia lesions in each type

As shown in Figure 2, in the present cohort, we decided to observe LM lesions classified as type I (72 lesions) every six months with dermoscopy. For the type II lesions (52 lesions), we did strict follow-up every three months with dermoscopy and, in cases in which the lesion enlarged during the follow-up period, we performed excisional biopsy (five lesions). The LM lesions classified as type III LM (13 lesions) were totally excised upon classification. In all the cases, complete surgical removal of the nail apparatus, including nail plate, nail bed, and nail matrix, was performed. The resulting defects were repaired with a split- or full-thickness skin graft.

Results

According to our clinical and dermoscopic criteria for LM lesions, of the 137 LM lesions, 72 were classified as type I and 52 as type II (Fig. 2). The other 13 were classified as type III (Fig. 2). None of the other 47 type II lesions showed significant enlargement or color change during the follow-up period. Thus, they were thought to be benign nevi/lentigo/functional melanonychia at end of the follow-up period.

Five type II LM lesions showed apparent enlargement during follow-up, and resection biopsy was performed (Fig. 2). Of the five LM lesions in which resection biopsy was done, three type II LM lesions showing a slightly increased number of melanocytes without atypia but with slightly enhanced melanin pigmentation in the nail matrix were histopathologically diagnosed as lentigo/benign melanocyte hyperplasia (Fig. 3). In contrast, two type II LM lesions revealed high melanocyte density and atypical melanocytes; in some, multinucleated melanocytes were seen in the nail matrix. These type II LM lesions were histopathologically diagnosed as MMIS. None of the other 47 type II lesions showed significant enlargement or color change during the follow-up period. Thus, they were thought to be benign nevi/lentigo/functional melanonychia at the end of the follow-up period.

All the type III lesions exhibited dense proliferation of melanocytes with moderate to severe atypia. Proliferating melanocytes were often confluent. Various levels of inflammatory cell infiltration were observed in the superfi-

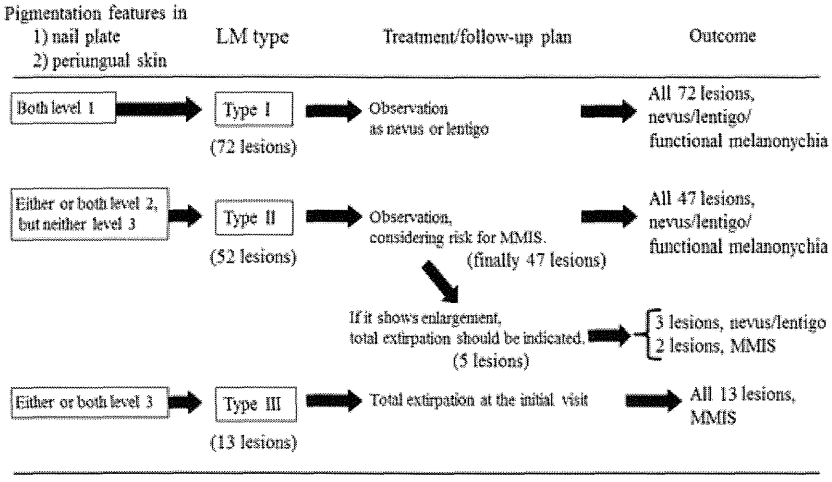

Figure 2 Classification criteria for longitudinal melanonychia (LM) types I–III and recommended treatment/follow-up plans. From pigmentation features in the nail plate and the periungual skin, LM lesions are classified into types I–III based on the level scoring shown in Table 1. Treatment/follow-up plans are observation as benign lesions (type I), observation considering malignant melanoma *in situ* (MMIS) risk (type II), and total excision (type III). In the present study, all 72 of the type I lesions were finally confirmed as benign. Only five of the 52 type II lesions showed size enlargement, and resection was done in these cases. Two of the five type II lesions that were resected proved to be MMIS. All 13 of the type III lesions were diagnosed as MMIS from histopathological examination

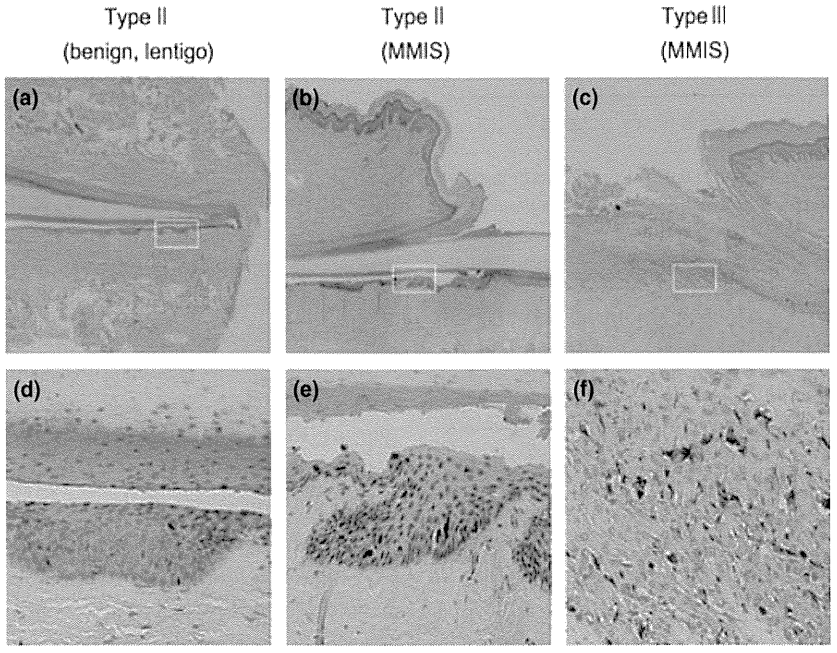

Figure 3 Histopathological features in the nail matrix portion of resected longitudinal melanonychia lesions. (a,d) A type II lesion finally diagnosed as lentigo. A slightly increased number of melanocytes and enhanced diffuse melanin pigmentation are seen in the nail matrix. Neither atypia of melanocytes nor inflammatory cell infiltration is observed. (b,e) Type II lesion, histopathologically diagnosed as malignant melanoma *in situ* (MMIS). Melanocyte density appears to be higher in the nail matrix than that seen in lentigo. The melanocytes show moderate atypia, and multinucleated melanocytes are found in the lesion. (c,f) MMIS lesion classified as type III. Proliferating melanocytes exhibit moderate to severe atypia. Slight inflammatory cell infiltration is seen in the upper dermis. The rectangles in a–c are enlarged in d–f. Hematoxylin and eosin stain; a–c: original magnification ×40; d–f: original magnification ×400

cial dermis. All these type III LM lesions were histologically diagnosed as MMIS.

Discussion

It is very difficult to make a clinical diagnosis of an LM lesion, because subungual MM must always be included in the differential diagnosis.[5] Various novel biopsy techniques applicable to LM have been introduced, and indications for different surgical approaches have been tried toward distinguishing MM from benign LM lesions.[5] Although the clinical evaluation of pigmented nail lesions has been refined and improved with the use of dermoscopy,[6,7] definitive diagnosis of LM can be made only by histopathological examination,[8] and it may not always be possible on a partial biopsy.[1] However, medical practitioners do not always resort to excisional biopsy of LM lesions, because it sometimes results in post biopsy nail dystrophy. To avoid such dystrophy, tangential biopsy (tangential matrix excision) has been recommended.[6] This technique is a transverse matrix biopsy modified to provide a very thin specimen (<1 mm thick). The tangential biopsy preserves everything necessary for complete nail regrowth and lowers the risk of post biopsy nail dystrophy.[6]

When we cannot exclude the possibility of MM completely, follow-up requires periodic medical examinations/visits and photographic and dermoscopic documentation[2]; in some instances, excisional nail biopsy should be done. In contrast, non-melanoma nail pigmentation and LM caused by benign melanocyte activation and lentigo need neither invasive investigations nor close follow-up.[2] To date, there is no consensus on modalities for the follow-up of pigmented bands in adults and children.[2] Particularly in children, it is very difficult to exclude the possibility of MM by clinical and dermoscopic examination alone. Although MM is reported to be rare in children, cases of nail matrix MMIS have been seen even in children.[2,9]

Levit *et al.*[10] summarized the noticeable features of subungual MM according to the ABCDEF criteria for subungual MM. A stands for *a*ge. B stands for brown to black *b*and with a breadth of 3 mm or more and variegated borders. C stands for *c*hange in the nail band or lack of change in nail morphology. D stands for the *d*igit most commonly involved. E stands for *e*xtension of the pigment on to the proximal and/or lateral nailfold (i.e., Hutchinson sign), and F stands for *f*amily or personal history of dysplastic nevus or MM. This ABC rule for clinical detection of subungual MM is practical and use-

ful. However, the overall accuracy of dermatologists in the diagnosis of nail matrix MMIS by clinical and dermoscopic evaluation is still low, and the definite diagnosis of subungual MM is made by means of a biopsy.[10,11]

In this study, we used clinical and dermoscopic criteria to classify 137 LM lesions into three types. After 1–8 years (median: 5.5 years) of follow-up, none of the type I lesions showed significant enlargement or color change. Neither the clinical nor the dermoscopic criteria changed for any of the type I lesions. Thus, all the type I lesions were thought to be benign. All the type III lesions were histopathologically confirmed to be MMIS. Five of the 52 type II lesions showed apparent enlargement and were resected. Two resected lesions were histopathologically diagnosed as MMIS and three as nevi/lentigo. None of the other 47 type II lesions showed significant enlargement or color change. Neither the clinical nor the dermoscopic criteria changed during the follow-up period for any of the 47 type II lesions, and they were thought to be benign. From these results, the type II lesions were considered to be in a gray zone that included both benign lesions and MMIS. Thus, we think type II lesions should be followed up every three months with dermoscopy, considering that MMIS can occur even in children, although type I lesions do not need strict follow-up and type III lesions should be excised as MM.

We think the proposed classification of LM lesions based on clinical and dermoscopic features is useful in deciding the treatment and follow-up for LM. However, in the present study, a biopsy was not performed for any of the type I lesions nor for the majority of type II lesions; the diagnosis of nevi/lentigo/functional melanonychia in such lesions was made by long-term clinical follow-up and was not confirmed histopathologically. We acknowledge that this reduces the scientific validity of the present study. Thus, further accumulation of LM cases with lesional histopathological examination will be needed to evaluate and confirm the reliability of these classifications, and modification should be done according to future studies.

References

1 Amin B, Nehal KS, Jungbluth AA, *et al.* Histologic distinction between subungual lentigo and melanoma. *Am J Surg Pathol* 2008; 32: 835–843.

2 Tosti A, Piraccini BM, de Farias DC. Dealing with melanonychia. *Semin Cutan Med Surg* 2009; 28: 49–54.

3 High WA, Quirey RA, Guillen DR, *et al.* Presentation, histopathologic findings, and clinical outcomes in 7 cases of melanoma in situ of the nail unit. *Arch Dermatol* 2004; 140: 1102–1106.

4 Ronger S, Touzet S, Ligeron C, *et al.* Dermoscopic examination of nail pigmentation. *Arch Dermatol* 2002; 138: 1327–1333.

5 Baran R, Kechijian P. Longitudinal melanonychia (melanonychia striata): diagnosis and management. *J Am Acad Dermatol* 1989; 21: 1165–1175.

6 Braun RP, Baran R, Le Gal FA, *et al.* Diagnosis and management of nail pigmentations. *J Am Acad Dermatol* 2007; 56: 835–847.

7 Hirata SH, Yamada S, Almeida FA, *et al.* Dermoscopy of the nail bed and matrix to assess melanonychia striata. *J Am Acad Dermatol* 2005; 53: 884–886.

8 Husain S, Scher RK, Silvers DN, *et al.* Melanotic macule of nail unit and its clinicopathologic spectrum. *J Am Acad Dermatol* 2006; 54: 664–667.

9 Iorizzo M, Tosti A, Di Chiacchio N, *et al.* Nail melanoma in children: differential diagnosis and management. *Dermatol Surg* 2008; 34: 974–978.

10 Levit EK, Kagen MH, Scher RK, *et al.* The ABC rule for clinical detection of subungual melanoma. *J Am Acad Dermatol* 2000; 42: 269–274.

11 Di Chiacchio N, Hirata SH, Enokihara MY, *et al.* Dermatologists accuracy in early diagnosis of melanoma of the nail matrix. *Arch Dermatol* 2010; 146: 382–387.